

Enhanced Cu^{2+} adsorption through double cross-linking of hydrogel with in situ CaCO_3

Yanqi Huang ^a, Bogdan V. Parakhonskiy ^{a, *}, Ales Lapanje ^b, Andre G. Skirtach ^{a, *}

^a Nano-Biotechnology Group, Faculty of Bioscience Engineering, Ghent University, 9000 Ghent, Belgium

^b Department of Environmental Sciences, Institut "Jožef Stefan", Jamova cesta 39, 1000 Ljubljana, Slovenia

* Correspondences: bogdan.parakhonskiy@ugent.be (B.V.P); andre.skirtach@ugent.be (A.G.S)

Abstract: Hydrogel systems formed with polymers possessing functional groups are widely explored for the removal of heavy metal ions due to their high adsorption capability, while numerous inorganic micro- nano-particles have been investigated as well due to their potential to bring in complementary properties to organic constituents. However, challenges still remain to design an efficient system for water purification. Here, a double cross-linked system with polyvinyl alcohol (PVA) and sodium alginate (SA) was developed by freeze-thaw cycles and Ca^{2+} -induced cross-linking. Importantly, calcium carbonate (CaCO_3) particles with a high adsorption capacity were doped via an *in-situ* method, which enhanced mechanical properties of PVA/SA hybrid films. Additionally, CaCO_3 doubled the Cu^{2+} adsorption efficiency of PVA/SA/ CaCO_3 compared to that of PVA/SA, and finally reached an adsorption equilibrium (A_e) of 95%. PVA/SA/ CaCO_3 experienced a typical pseudo-second-order adsorption kinetic model and the Langmuir model of adsorption isotherm, indicating that the adsorption process was more inclined to monolayer chemisorption. The adsorption thermodynamic revealed that the adsorption process was spontaneous and exothermic. The highly efficient adsorption of Cu^{2+} ions by PVA/SA/ CaCO_3 was the result of the synergistic adsorption mechanism of electrostatic interaction, complexation, cation exchange and ionic reaction. Regeneration experiment and comparative results shows that PVA/SA/ CaCO_3 has greater application potential for wastewater purification.

Key words: wastewater purification, PVA/SA/ CaCO_3 , mechanical properties, adsorption efficiency, adsorption kinetic

1. Introduction

Effective treatment of industrial wastewater plays a crucial role in the environment and human health. In particular, heavy metal ions are difficult to degrade and highly toxic, leading to water eutrophication and ecological imbalance [1–3]. Through the bioaccumulation and in several cases by the biomagnification processes, these pernicious ions can be transferred to the human body via the food chain, resulting in chronic poisoning and organ damage [3–5]. In order to achieve the goal of water purification, the key is to obtain a material that can efficiently remove heavy metal ions. The commonly used adsorbents include zeolite, activated carbon, mesoporous silicon dioxide, biomass, *etc*, characterized by their charge and high porosity properties to complete the adsorption of target ions [2,3,6–8]. However, some of them suffer from problems of low adsorption capacity and secondary pollution, and more efficient and practical candidates are urgently demanded [9].

In recent years, there has been a growing interest in utilizing hydrogels and their derivatives in purification systems [10,11]. Most of them are eco-friendly and possess unique functional groups, such as carboxyl and amino groups, which facilitate interactions with metal ions through crosslinking, complexation, and electrostatic attraction, so as to achieve higher removal effects [12]. For example, sodium alginate (SA), a natural polysaccharide, exhibits remarkable cross-linking properties and contains metal ion binding sites (-OH, -COOH), which makes it easy to cross-linking with metal cations to form hydrogels, and is widely applied in the removal of heavy metals by adsorption [13,14]. However, the application potential of single-component SA hydrogel is limited by their relatively low mechanical properties, especially the low elasticity of SA thin films formed via ionic cross-linking, making them extremely vulnerable to damage under applied load [15]. In this regard, polymer blending provides a promising approach to develop composite materials with superior performance. Polyvinyl alcohol (PVA) is considered to be a representative with excellent mechanical properties and biocompatibility [16]. It can be modified by various methods, including freeze-thaw cycles,

chemical cross-linking using cross-linking agents, and external stimuli such as light and heat to obtain PVA-based materials with high strength and elasticity, and excellent film-forming abilities [16]. Moreover, PVA is susceptible to hydrolysis under certain conditions, allowing it to degrade in the environment, which makes PVA potential for applications in disposables, packaging products and environmentally friendly solutions [17,18]. Consequently, PVA can serve as a highly suitable candidate for development of environmentally friendly composite materials for the heavy metal adsorption [4,16,17,19–22]. For example, Zhang et al [4]. prepared PVA/SA hydrogel with high removal efficiency for Pb (II) and Cr (VI). Chen et al [23]. used glutaraldehyde cross-linking to prepare a PVA/SA/Cr (III) porous membrane with efficient selective adsorption capacity for Cr. The graphene oxide encapsulated PVA/SA hydrogel microspheres prepared by Yi et al. showed high Cu (II) and U (VI) removal efficiency [24]. The magnetic PVA/SA microspheres obtained by Zhang et al. had selective adsorption of aromatic compounds [25].

Taking inspiration from hybrid inorganic micro- nano and particle adsorbents such as mesoporous SiO₂, Fe₃O₄, and zeolite, the presence of vaterite is worth noting due to its high loading efficiency in drug delivery systems, which underscores its effectiveness as an excellent adsorbent [26–29]. Vaterite, a polymorph phase of CaCO₃, typically has a predominantly spherical shape with porosity of up to 40% [30]. It can be easily synthesized through chemical reactions at close to room temperatures or in the presence of organic additives, and its favorable biocompatibility, loading properties, filtrability and fillibility make it a cost-effective and versatile material with multifunctional applications, including drug delivery systems, fillers and absorbents [13,31–37]. Furthermore, the interaction between carbonate and heavy metal ions will form carbonates with low solubility, which will greatly improve the adsorption effect of particles on heavy metal ions, thereby achieving the purification effect [38,39]. Therefore, compounding CaCO₃ into PVA/SA polymer to form composite materials for heavy metal ion adsorption is regarded as a good strategy. For example, Stanley revealed that CaCO₃-enhanced PVA/SA hydrogel has higher urea encapsulation efficiency than PVA/SA gel

[40]. The PVA/CaCO₃ adsorbent prepared by Jahani et al. showed good adsorption efficiency for cationic dyes [41]. Tang et al. doped CaCO into SA/chitosan hybrid hydrogel to prepare excellent adsorption capacity for a variety of heavy metal ions [42]. More studies were summarized in subsequent comparative studies.

Accordingly, in this work, a double cross-linked interpenetrating hydrogel film made of SA and PVA was prepared and used to explore its ability to adsorb and remove Cu²⁺ ions. In addition, different concentrations of CaCO₃ phases were introduced during the composite film synthesis process by in situ synthesis method, and the influence of the presence of CaCO₃ on the mechanical properties of the film and the Cu²⁺ adsorption capacity was explored. By examining the adsorption amount of Cu²⁺ in the film at different time dimensions, temperatures, and using various characterization methods to complete the analysis of the surface structure and phase composition of the film, the adsorption mechanism of Cu²⁺ is further evaluated. These results will provide support for the application of the composite membrane material in water purification.

2. Experimental

2.1. Materials and chemicals

All chemical materials were purchased from Sigma Aldrich without any further purification, unless specially mentioned. Sodium carbonate (Na₂CO₃, ACS reagent) and calcium chloride dihydrate (CaCl₂·2H₂O, ≥ 99.0%) were used to synthesize CaCO₃ particles, poly(vinyl alcohol) (PVA, fully hydrolyzed, 11-14 cps, 4 % in H₂O (20 °C)(lit.)) and alginic acid sodium salt (SA, viscosity of 2% solution at 25 °C: 250 cps) were used to prepare hydrogels. Copper sulfate (CuSO₄, reagent plus, ≥ 99%) were selected to prepare Cu²⁺ ionic solution with designed concentrations to simulate waste-water. Ethylenediamine tetra acetic acid (EDTA, reagent grade, 98.5-101.5% (titration)) was used as chelating agent to facilitate the measurement of Cu²⁺ complex, and finally calculate the content of Cu²⁺ in the solution. Milli-Q water (18.2 MΩ·cm) was acted as solvent in all process.

2.2. Preparation of PVA/SA/CaCO₃ hybrid films

First, 10 g of PVA powder was weighed and dissolved in distilled water under stirring at 80 °C for 2h to

obtain a 100 mg/mL of PVA solution. 0.5 g of SA powder was weighed and dissolved in distilled water under stirring at 40 °C for 1h to obtain a 10 mg/mL of SA solution. According to the designed concentration (0.1-1 M), Na₂CO₃ was weighed and added to 5 mL SA solution until it was completely dissolved, and then an equal volume of PVA solution was added and stirred at room temperature for 1h to make all components fully mixed. After that, 5 mL of CaCl₂ solution (pH of 8.0 ± 0.2) (0.1-1 M) with an equal concentration of Na₂CO₃ was added dropwise to the mixture with a rotation speed of 1000 rpm at room temperature, and the solution turned milky white, which indicated the formation of CaCO₃. After 5 min, 0.75 mL of the suspension was pipette into a 24-well plate, followed by 5 freeze-thaw cycles (freezing temperature is -20 °C, thawing at room temperature), and then 0.3 M CaCl₂ solution with pH of 8.0 ± 0.2 (1mL) was added to induce SA cross-linking for 1h (1mL). Finally, the cross-linked hybrid hydrogel sheets were washed with distilled water and dried in an oven (40 °C) for subsequent experiments. (**Fig. 1**).

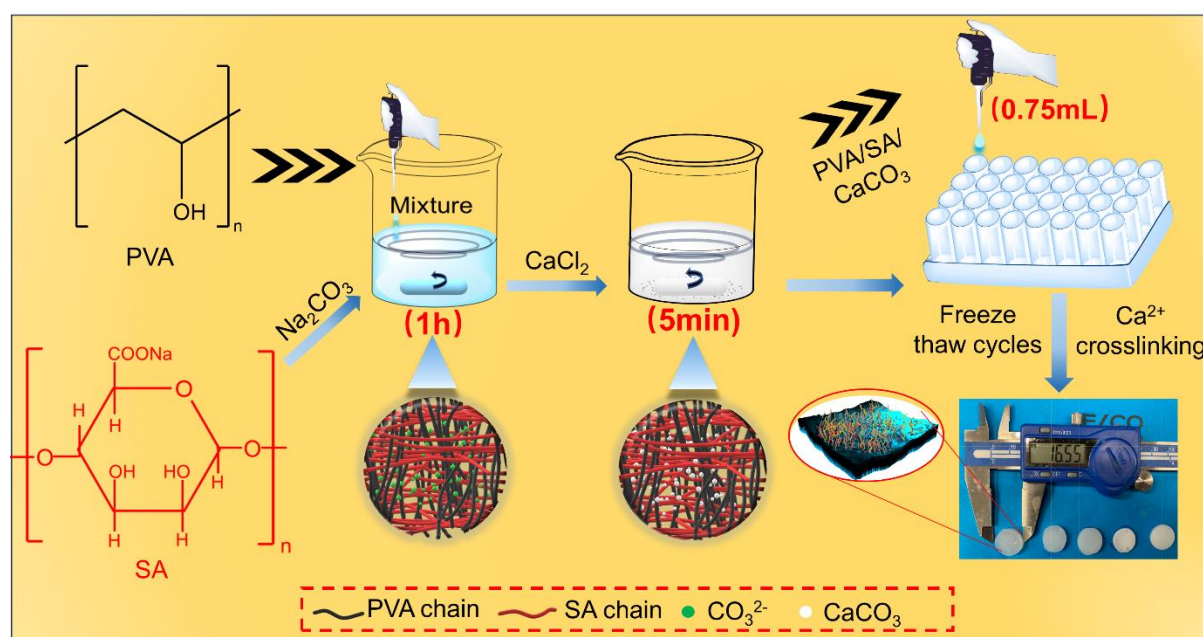


Fig. 1. Fabrication flow chart and images of PVA/SA/CaCO₃ hydrogel sheets.

2.3. Swelling and biodegradability analysis of PVA/SA and PVA/SA/CaCO₃ hybrid sheets

The dried mass (M_0) of the sheets was measured after they were completely dried. Then, the sheets were immersed in deionized water and kept at room temperature for 48 h until the sheet reached a constant weight,

and then they were weighted (M_w). The swelling rate (S) can be calculated using Eq. (1):

$$S (\%) = \frac{M_w - M_0}{M_0} \times 100\% \quad (1)$$

where M_w and M_d are the mass of swelling and dried sheet, respectively, five parallel tests were selected for each type of sample.

The dried samples were placed in neutral water, a high-concentration ion solution (1M NaCl), and a pH 10 buffer solution for 48 hours, respectively. The mass (M_1) was obtained after drying, and the biodegradability rate (D) can be calculated using Eq. (2):

$$D (\%) = \frac{M_0 - M_1}{M_0} \times 100\% \quad (2)$$

2.4. Mechanical properties of hybrid films

The tensile strength of hybrid films was measured by universal testing machine (UTM-3, LS1 Series) with the NEXYGENPlus software. All swollen film samples were cut into strips that can be mount in the device. After the sample was mounted on the fixture, the effective length, width and thickness of the sample were measured using a vernier caliper. Tensile tests were done at an extension rate of 100 mm/min.

2.5. Adsorption experiments

Cu^{2+} solution with a concentration of 0.002, 0.005, 0.01, 0.02, 0.05, 0.1 M was prepared. To prevent the dried hydrogel sheets from reducing the volume of the medium during the adsorption process, each piece of sheet with 45 ± 5 mg firstly completed the absorption of water. Then, 1 mL of Cu^{2+} solution was subsequently added to the well containing the swollen sheet, and ensured that the sheet was completely submerged. A time series and different temperatures (4 °C, 20 °C, and 40 °C) were designed. After completing the adsorption process, the suspension was pipetted into 2-mL Eppendorf tube and centrifuged to remove possible residual film debris. Then, the buffer (0.1 mL) and EDTA (0.2 mL) was added dropwise to the solution and placed it in a boiling water bath for 2 min to promote the formation of Cu^{2+} complexes. Finally, using UV-vis spectrophotometer to measure the adsorption peak intensity at a wavelength of 734 nm, and the remaining

Cu^{2+} content in the solution was calculated according to the Cu^{2+} calibration curve. The adsorption capacity (q_t) and adsorption efficiency (Ae) of the film were calculated as follow [43]:

$$q_t = \frac{(C_0 - 1.3 \times C_t) \cdot V}{M} \quad (3)$$

$$Ae (\%) = \frac{(C_0 - 1.3 \times C_t)}{C_0} \times 100\% \quad (4)$$

where q_t ($\text{mg} \cdot \text{g}^{-1}$) is the amount of Cu^{2+} adsorbed per gram, C_0 is the initial Cu^{2+} concentration and C_t is the Cu^{2+} concentration of suspension after t time adsorption, V (L) is the volume of the solution, M (g) is the mass of beads. The coefficient 1.3 represents the volume of the tested supernatant (1.3mL: 1mL + 0.1mL of buffer + 0.2 mL of EDTA) relative to the volume of the initial solution added (1ml).

2.6. Characterization of PVA/SA and PVA/SA/ CaCO_3 hybrid films

The surface morphologies of the hybrid sheets before and after adsorption tests were observed using Scanning Electron Microscopy (SEM, JEOL, Japan), and each sample was fully dried at 40 °C and coated with thin gold film by Sputter coating before the measurements. The three dimensions (3D) surface images and surface roughness of the initial samples was detected by Atomic Force Microscopy (AFM), Nanowizard 4TM (JPK bioAFM, Bruker) in the contact mode using a DNP-S10 (Budget Sensor) cantilever and the set-point of 0.5 nN. Fourier Transform Infrared (FTIR, Vertex 70 Bruker) spectroscopy (in the wavelength range from 400 cm^{-1} to 4000 cm^{-1} with a resolution of 1 cm^{-1}) was used to analyze the structure of PVA/SA and PVA/SA/ CaCO_3 sheets, and the infrared spectra of each sample were analyzed using OPUS software. X-ray diffraction (XRD, Rigaku) was used to analyze the phase composition of all samples. All measurements were made with a Rigaku Mini-flex diffractometer (Rigaku, Japan) by using a Cu K α ($\lambda = 0.154$ nm) radiation source at 45 kV and 200 mA in the scanning angle range from 10° to 80° with the speed of 0.1°/s.

3. Results and discussion

3.1. Swelling and biodegradability properties

The swelling rate of the samples decreased with the increase of CaCO_3 content, and it was as high as

250% in PVA/SA hydrogels, while only half amount in the hybrid sheet containing 0.7 M CaCO_3 (**Fig. S1**). Obviously, the existence of a large number of hydroxyl and carboxyl groups in PVA and SA is the key to affect the swelling rate of hybrid hydrogels. It is well-known that hydrogen bonding occurs between water molecules and carboxyl and hydroxyl groups, leading to the formation of a hydration shell on the gel surface, which can enhance the capacity to absorb and retain water molecules. In addition, the dense network structure formed by the double crosslinking system of PVA and SA will also enhance its interception effect on water molecules. In contrast, CaCO_3 primarily adsorbs water molecules through van der Waals forces, which are relatively weaker compared to hydrogen bonding. Additionally, the increased amount of CaCO_3 in hybrid hydrogels reduced the effective content of PVA and SA, as well as the network structure of the gel film, thereby diminishing its water-holding ability. The biodegradability results showed that the composite had no significant mass loss in these medium, indicating that the composite would not degrade or flake off during the adsorption process in a non-acidic environment, thus preventing the possibility of secondary pollution.

The addition of CaCO_3 resulted in a decrease in the tensile strength of the film, primarily due to the disruption of the tight double cross-linked network structure formed by PVA and SA, especially at higher particle concentrations (0.5 - 0.7 M). At these concentrations, micro-nanoparticles tended to aggregate, leading to localized defects such as pores, cracks, and irregular arrangement of polymer molecular chains, thus weakening the overall strength of the film. However, the elongation of the film significantly improved with the introduction of CaCO_3 , particularly at a concentration of 0.3 M, where the maximum strain doubled compared to PVA/SA alone (**Fig. S2**). This increased strain energy allows the film to absorb more energy before failure, as the particles aid in dispersion toughening and act as bridges in the three-dimensional network due to electrostatic attraction and bonding with polymer groups. As a result, a reasonable particle concentration is crucial to balance the strength and toughness of the material.

3.2. Characteristics of PVA/SA and PVA/SA/ CaCO_3 sheets before and after metal adsorption

3.2.1. Surface morphology

The freeze-dried sample showed a porous skeleton structure (**Fig. S3**), the particles were distributed on the polymer skeleton when the CaCO_3 content was low, but as the CaCO_3 content increased, a large number of particles were filled in the pores of polymer skeleton, which also caused the decrease of porosity of the composite (**Fig.S3d-e**), **Table S1**). Since the samples used for adsorption experiments were dry samples, we also characterized them, as shown in **Fig. 2**. Except for the PVA/SA sample, there was a significant formation of spherical particles in PVA/SA/ CaCO_3 samples. Given the strong interaction between Ca^{2+} and CO_3^{2-} ions, as well as the typical morphology and synthesis conditions, this implied that a large amount of vaterite was formed within the PVA/SA/ CaCO_3 sheets, which was proved by the IR and XRD spectra (**Fig. 4**). The number of particles increased significantly with the increase of the concentration of initial solutions (CaCl_2 and Na_2CO_3), while the size of vaterite decreased. Obviously, the existence of PVA and SA greatly prevented the phase transition from vaterite to calcite and inhibited excessive growth of crystals, since they could cover the surface of vaterite at the moment of its formation through electrostatic interaction [44]. In addition, the hydrogen bonds formed between hydroxyl and carboxyl groups in the polymer, along with the ions on the vaterite surface and the steric hindrance effect group formed on vaterite, hinder particles aggregation and dissolution, thereby delaying or preventing the recrystallization and phase transition of vaterite process [44,45]. The increase of concentration improved the interaction between solute and solute, as well as solute and solvent, which increased the nucleation rate on the one hand, and limited the aggregation between molecules on the other hand. During nucleation formation, the wrapping of organic matter restrained particle growth.

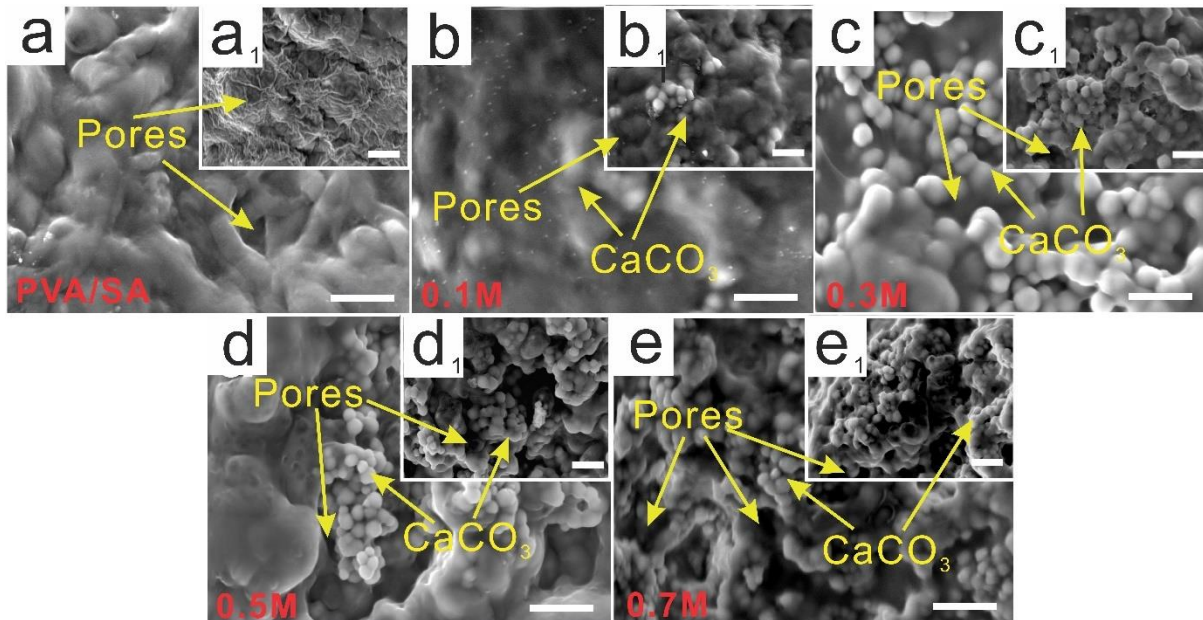


Fig. 2. Surface morphologies PVA/SA and PVA/SA/CaCO₃ hydrogels sheets with different CaCO₃ concentration before (a-e) and after (a₁-e₁) adsorption tests. (The scale bar in all panels is 10 μm).

Interestingly, the surface of these dried sheets showed different level of flatness. The surface of PVA/SA without vaterite had obvious wrinkles, attributed to the uneven evaporation of moisture during the drying process. With the addition of small amounts of CaCO₃, the surface of the hydrogel sheets became smoother (PVA/SA/0.1M CaCO₃). However, when the concentration of CaCO₃ was too high (≥ 0.5 M), an uneven structure appeared, characterized by the accumulation of particles and an increase of local pits. Apparently, the agglomeration effect caused by excess vaterite exceeded the mutual repulsion between particles, hindering liquid flow during solvent volatilization in the polymer solution with high viscosity, thus increasing defects of the hydrogel sheets.

The surface fluctuation states of different hydrogels after swelling were accurately obtained by selecting an appropriate cantilever through contact mode, as shown in **Fig. 3**. As expected, compared to the sample containing CaCO₃, PVA/SA had a relatively smooth surface with an average roughness (Ra) of 287.2 nm. When CaCO₃ was introduced, there were obvious high points and valleys on the surface. However, compared to samples with a low concentration of 0.1 M and a high concentration of 0.7 M, the surface fluctuations of

0.3 and 0.5 M samples were less dazzling, indicating that the latter had flatter surfaces due to an appropriate filling of CaCO₃ particles. When the content of CaCO₃ particles was too low or too high, the hydrogel exhibited obvious convex in the local area due to uneven distribution and agglomeration, which may show inaccurate roughness information (the light-colored part of **Fig.3 a1-e1**). The influence of roughness on the adsorption efficiency is multifaceted. Higher surface roughness leads to higher surface area, which in turn provides more adsorption sites for the adsorption of heavy metal ions. On the other hand, roughness can affect the distribution of surface charge, for example, the charge will be concentrated at the tip, thus changing the adsorption of ions on the surface. Typically, it was found that the raised part of the film had a darker color during the experiment. Nonetheless, it is important to note that although a rough surface facilitates heavy metal ion adsorption, uneven particle distribution can compromise the mechanical properties of the film, posing a challenge to consider.

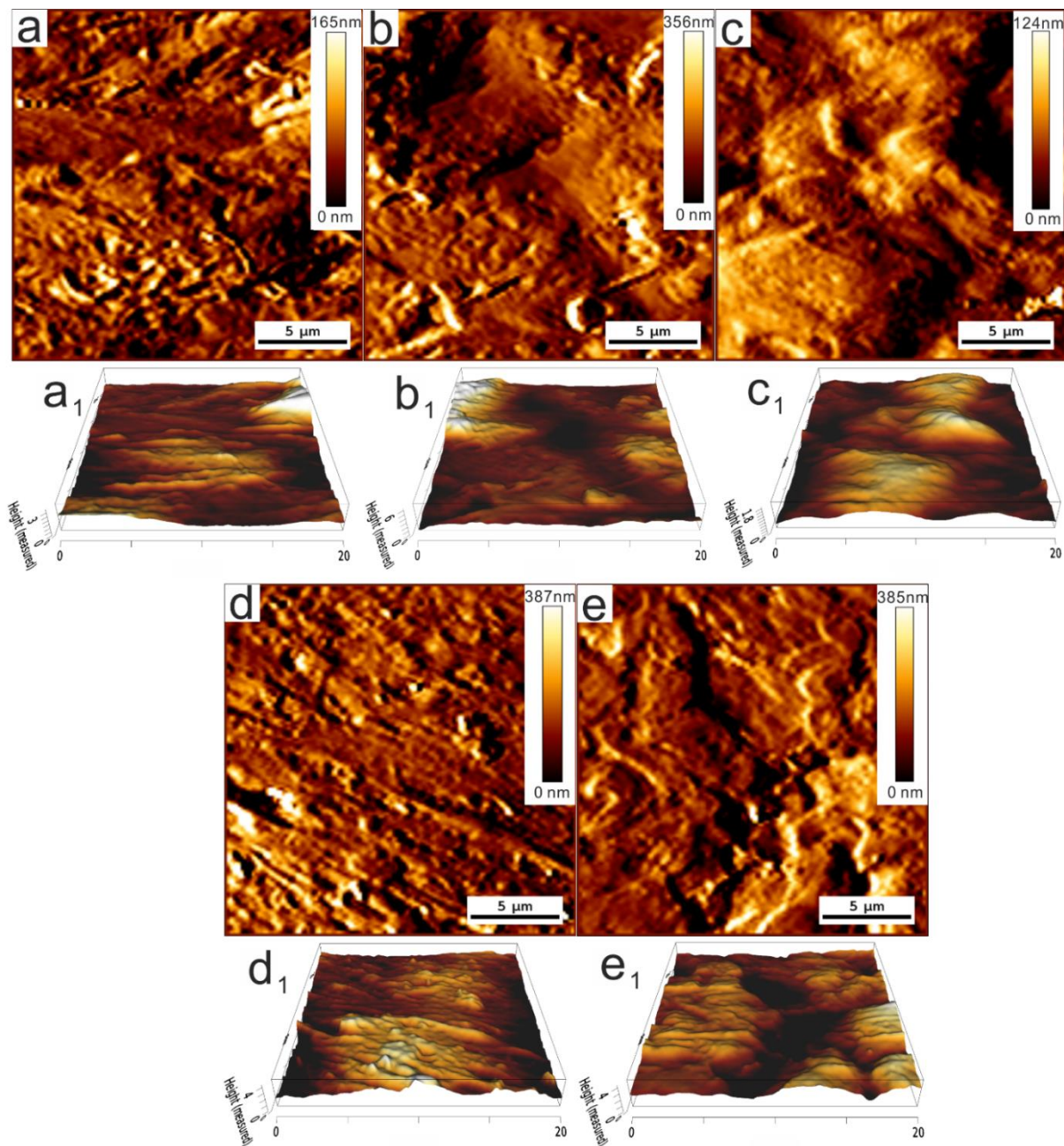


Fig. 3. Three dimensions (3D) surface images of PVA/SA (a) and PVA/SA/CaCO₃ hydrogels sheets with different CaCO₃ concentration (b) 0.1 M, (c) 0.3 M, (d) 0.5 M, (e) 0.7 M before adsorption tests.

3.2.2. Phase composition

Fig. 4a shows the infrared spectra of PVA/SA and PVA/SA/CaCO₃ hydrogel sheets. All samples showed a strong vibration absorption peak at 3290 cm⁻¹, which was attributed to the stretching vibration of -OH in PVA and SA. These peaks shifted as the CaCO₃ content increased. Absorption peaks caused by -CH and -C-O stretching were observed at 2909 cm⁻¹ and 1085 cm⁻¹, and the COO⁻ vibration absorption peak also appeared

at 1412cm^{-1} . In PVA/SA/ CaCO_3 hydrogel sheets, the $-\text{COO}-$ stretching band shifted to higher wavenumbers, implying the formation of ionic bonding between Ca^{2+} and $-\text{COO}-$. The characteristic bands at 848 cm^{-1} (out-of-plane deformation (2)) and 743 cm^{-1} (in-plane deformation (4)) confirmed the presence of vaterite in PVA/SA/ CaCO_3 .

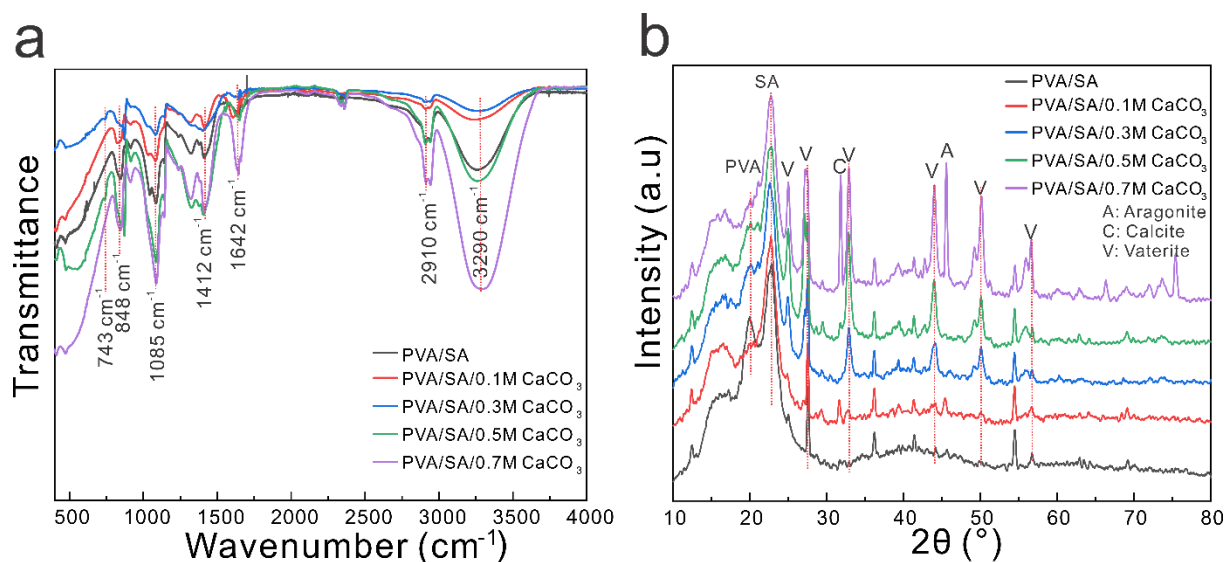


Fig. 4. IR and XRD spectra of PVA/SA and PVA/SA/ CaCO_3 with different concentrations of CaCO_3 hydrogel sheets.

Fig. 4b shows XRD patterns of PVA/SA and PVA/SA/ CaCO_3 . XRD patterns of crosslinked PVA and SA hydrogels exhibited broad and weak diffraction peaks due to the strong intermolecular and intra-molecular hydrogen bonding between polymer chains after crosslinking process. Prior to this, we tested the XRD patterns of crosslinked PVA hydrogels and Ca^{2+} crosslinked SA hydrogels, respectively (**Fig. S4**), and found that PVA had strong diffraction peaks at $2\theta=19.95^\circ$ and 22.98° , indicating that PVA had high crystallinity. While the SA mainly showed strong peaks at $2\theta=16.2^\circ$ and 22.8° . Comparison PVA/SA and PVA/SA/ CaCO_3 with these two initial hydrogels, it was found that in PVA/SA, the peak at $2\theta=22.9^\circ$ was significantly enhanced, which might be the result of overlapping effect and the interaction between $-\text{OH}$ in PVA and $-\text{COOH}$ in SA. However, with the increase of CaCO_3 content, the peak of PVA at $2\theta=19.95^\circ$ significantly impaired, indicating that the crystallinity of PVA decreased, this would result in lower mechanical properties. On the other hand, the appearance of diffraction peaks at $2\theta=32.9^\circ$, 44.02° , 50.13° and 55.92° confirmed the formation of vaterite,

which was consistent with the spherical particles appearing in the SEM images, and with the increase of the initial Ca^{2+} concentration, the corresponding diffraction peaks intensity of vaterite increased significantly.

3.3. Adsorption analysis of Cu^{2+} by PVA/SA/ CaCO_3 hybrid hydrogel sheets

3.3.1. Effect of CaCO_3 concentration on the Cu^{2+} adsorption efficiency of hydrogel sheets

The Cu^{2+} adsorption efficiency of PVA/SA/ CaCO_3 hydrogel sheets containing different concentrations of CaCO_3 is shown in **Fig. 5(a-c)**. The content of CaCO_3 had a significant impact on the Cu^{2+} adsorption efficiency of the hybrid sheets, especially compared with PVA/SA. For example, even with the addition of 0.1 M CaCO_3 , the adsorption efficiency of hybrid sheets increased by 50% compared with that of PVA/SA before reaching saturated adsorption, even up to twice the saturated adsorption efficiency of PVA/SA. However, the Cu^{2+} adsorption efficiency did not increase proportionally to the increase of CaCO_3 content. At the beginning of the adsorption (15 min) and the middle of the adsorption (60 min), when the concentration of CaCO_3 was 0.3 M, the Cu^{2+} adsorption efficiency of PVA/SA/0.3 M CaCO_3 reached the peak, and then decreased with the increase of CaCO_3 , this result was especially significant at 4°C and 20°C. This suggests that the adsorption rate of Cu^{2+} by hybrid hydrogels initially rises and then declines with increasing CaCO_3 content. This phenomenon may stem from an excessive amount of CaCO_3 altering the structure and surface characteristics of the polymer, such as surface charge or pore structure. Additionally, excessive CaCO_3 may form a coating on the hydrogel surface, impeding Cu^{2+} contact with the polymer's adsorption sites, thereby diminishing the Cu^{2+} adsorption rate to some extent. However, in the presence of CaCO_3 , its content did not significantly affect the saturation adsorption efficiency of PVA/SA/ CaCO_3 hydrogel sheets. It is worth noting that even though the adsorption efficiency of PVA/SA/0.7 M CaCO_3 was equivalent to that of PVA/SA at the initial period (15 min), but the former gradually exceeded (60 min) the latter and final significantly exceeded (900 min), which meant that CaCO_3 accelerated the adsorption rate, which was more obvious at 20 and 40 °C. In this case, the increase of CaCO_3 concentration significantly improved the Cu^{2+} adsorption efficiency in the unsaturated

section, especially from 0 to 0.5 M, but slightly decreased at 0.7M. However, the saturation adsorption efficiency of all PVA/SA/CaCO₃ was almost equal. This was because over 90% of the Cu²⁺ in the solution was adsorbed by PVA/SA/CaCO₃, leading to a high concentration difference effect that made it difficult for PVA/SA/CaCO₃ to further demonstrate variability. Alternatively, the incorporation of only a small amount of CaCO₃ may result in an excessive number of adsorption sites in PVA/SA/CaCO₃ relative to Cu²⁺, thereby exhibiting up to 90% adsorption efficiency in all samples.

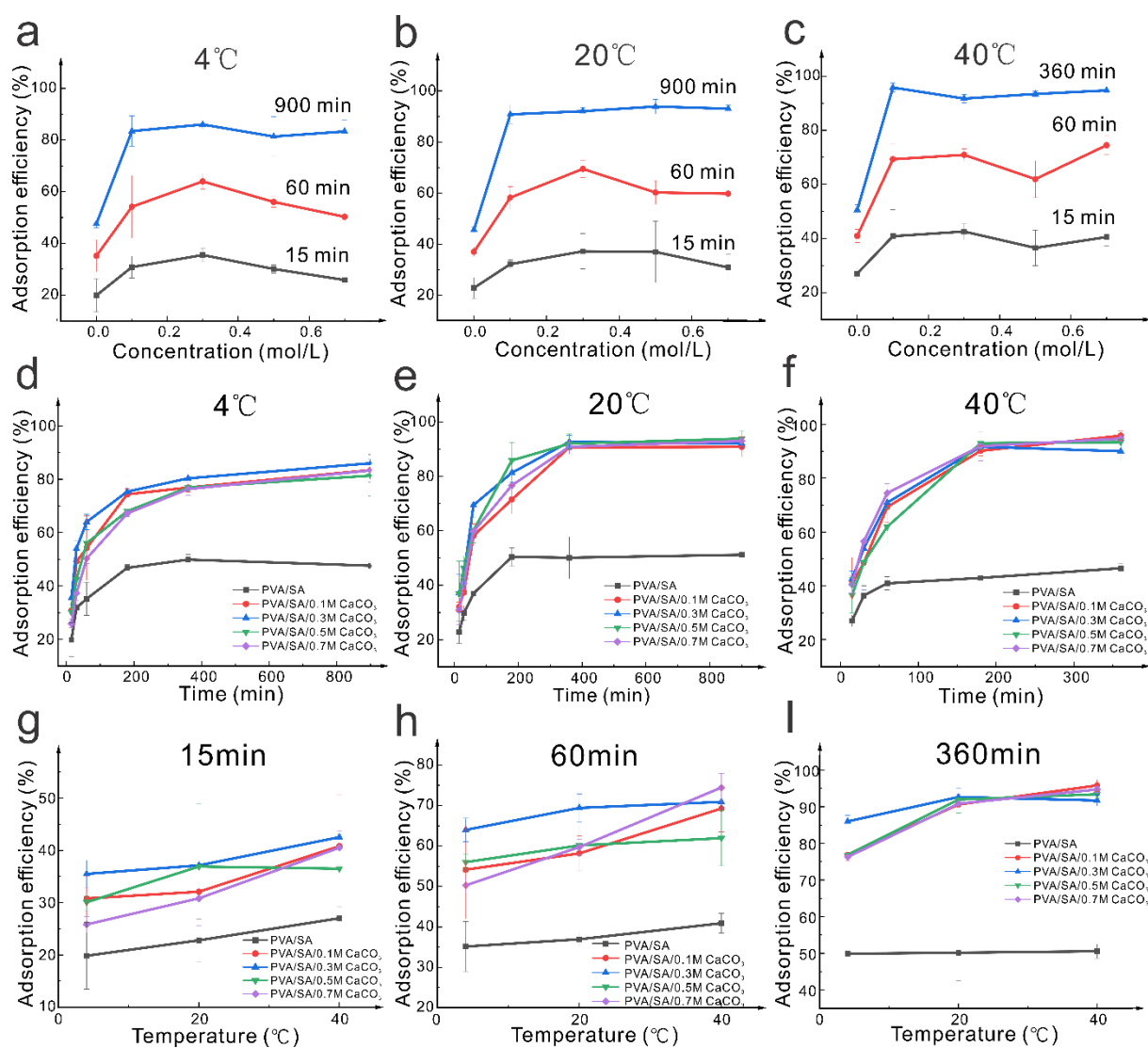


Fig. 5. Cu²⁺ adsorption efficiency of PVA/SA and PVA/SA/CaCO₃ hydrogel sheets (a-c) as a function of CaCO₃ concentration; (d-f) as a function of time; (g-i) as a function of temperature.

3.3.2. Effect of time on the Cu²⁺ adsorption of hybrid films

The adsorption efficiency of PVA/SA and PVA/SA/CaCO₃ hydrogel sheets at three temperatures with time interval is shown in **Fig. 5(d-f)**. The influence of time on the adsorption efficiency of the sample was significant, especially in the early stage of adsorption process. At 4 °C, the growth rate of adsorption efficiency of all samples in the first 1h was very fast, during which the adsorption efficiency of PVA/SA increased from 19 ± 6% (15 min) to 32 ± 5% (1 h), while that of PVA/SA/CaCO₃ directly became almost twice. Subsequently, the adsorption rate gradually slowed down until it approached the adsorption equilibrium at 6 h. Similar curves of adsorption efficiency with time also appeared at other temperatures. Obviously, the sample adsorbed more Cu²⁺ with the extension of time, in that case, the difference of ion concentration between the sample surface and the solution gradually decreased, thus diminishing the driving force of ion diffusion, and finally manifested in the decrease of adsorption rate and the appearance of adsorption equilibrium state. The influence of time became more significant with the increase of temperature. Compared with 4 °C and 20 °C, the adsorption rate of PVA/SA accelerated significantly, which showed that the slope of the adsorption curve was steeper in the early period (15 min- 1 h) and reached the adsorption equilibrium state almost in 3 h.

3.3.3. Effect of temperature on the Cu²⁺ adsorption of hybrid films

The adsorption efficiency of PVA/SA and PVA/SA/CaCO₃ hydrogel sheets at three adsorption intervals with temperatures is shown in **Fig. 5(g-i)**. It can be seen that the influence of temperature was different in three adsorption periods. Before reaching the adsorption equilibrium, the increase of temperature significantly expedited the Cu²⁺ adsorption of the hydrogel sheets regardless of the absence of CaCO₃. The slope of the curve indicated that their growth rates were different, except for PVA/SA whose slope of the adsorption and temperature curve was constant. When the temperature rose from 20 °C to 40 °C, the slope of the curve increased, indicating that the adsorption rate of the sample was accelerated, which was closely related to the molecular thermal motion. However, at adsorption equilibrium (360 min), the increase of temperature did not cause changes of PVA/SA, and its final adsorption efficiency remained at about 50% at three different

temperatures. The introduction of CaCO_3 broke the low adsorption equilibrium of PVA/SA, and the adsorption amount of PVA/SA/ CaCO_3 at 20 °C was significantly higher than that at 4 °C. But continuing to increase the temperature to 40°C did not achieve higher adsorption effect. Because the adsorption efficiency of the hydrogel sheet had reached about 90% at that moment, and the concentration of Cu^{2+} on the surface of the sample was greatly higher than that in the solution, which made the initial driving force from the solution to the sample surface generated from the concentration difference became reversed, preventing the further adsorption procedure of Cu^{2+} . The equilibrium adsorption of Cu^{2+} increased with the increase of temperature, indicating that the adsorption is an endothermic process. Strictly speaking, the ability to achieve such a high metal ion adsorption efficiency can be called an excellent water purifier.

3.3.4. Adsorption kinetics of PVA/SA and PVA/SA/ CaCO_3 hydrogel sheets

In view of the similar adsorption curves of PVA/SA/ CaCO_3 hydrogel sheets containing different concentrations of CaCO_3 , PVA/SA/0.3M CaCO_3 was selected to study the adsorption kinetics and compare with PVA/SA, and both pseudo-first-order and pseudo-second-order kinetic models were used to fit the adsorption process, as shown in **Fig. 6**. **Table 1** presents the pseudo-order coefficients for the kinetic models of Cu^{2+} adsorption onto the hydrogel sheets, indicating that the correlation coefficient for the second-order reaction involving the entire Cu^{2+} complex was closer to 1 compared to the first-order reaction, and the calculated A_e value was closer to the experimental value. These results suggest that the pseudo-second-order kinetic model was more suitable for describing the adsorption process of Cu^{2+} onto PVA/SA and PVA/SA/ CaCO_3 hydrogel sheets, indicating that the adsorption process was chemisorption-dominated rather than simple physical adsorption. This observation also aligned with the functional groups present in PVA/SA/ CaCO_3 . In this case, the carboxyl functional group interactions between PVA/SA and Cu^{2+} play a major role, while the CO_3^{2-} ions generated by CaCO_3 in PVA/SA/ CaCO_3 had a significant impact on the adsorption process, since CO_3^{2-} possesses stronger charge properties compared to carboxyl groups, it

preferentially binds to Cu^{2+} to form more stable compounds, which was why PVA/SA/ CaCO_3 exhibited higher adsorption capacity. Accordingly, the Cu^{2+} ions adsorption of PVA/SA and PVA/SA/ CaCO_3 hydrogels sheets is controlled by diffusion and reaction rate, and thus is a chem-physical adsorption. The equation for Pseudo-first-order and Pseudo-second-order kinetics were introduced initially by Lagergren [46], and now we generally use the form proposed by Ho and McKa [47].

$$\text{Pseudo-first-order: } q_t = q_e(1 - e^{-k_1 t}) \quad (5)$$

$$\text{Pseudo-second-order: } q_t = \frac{K_2 q_e^2 t}{(1 + K_2 q_e t)} \quad (6)$$

Where q_t ($\text{mg} \cdot \text{g}^{-1}$) is the adsorption capacity of samples at time of t , q_e ($\text{mg} \cdot \text{g}^{-1}$) is the value of equilibrium, K_1 (min^{-1}) and K_2 ($\text{g} \cdot \text{mg} \cdot \text{min}^{-1}$) are the rate constants for the Pseudo-first order and Pseudo-second-order models respectively.

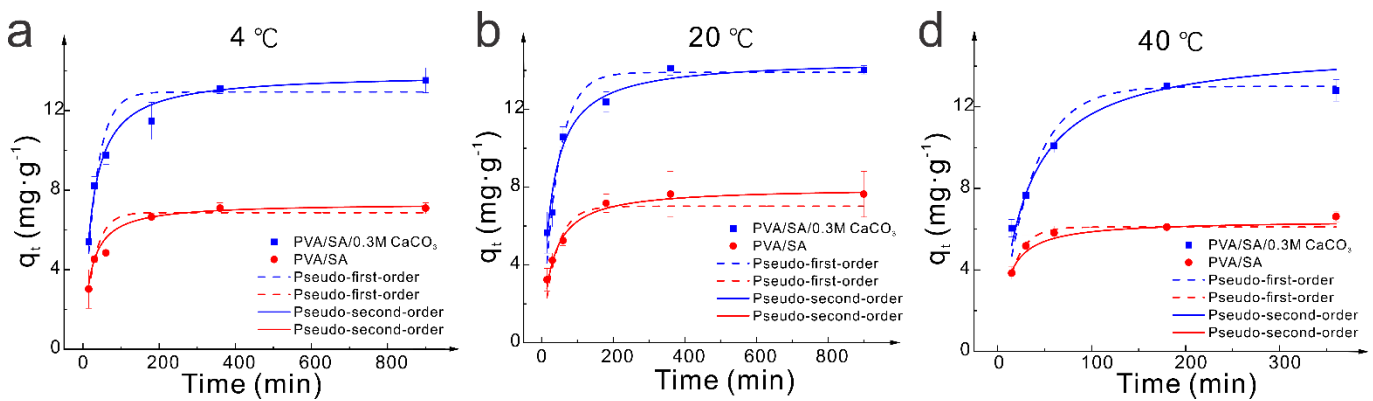


Fig. 6. Adsorption kinetics (pseudo-first-order and pseudo-second-order models) of PVA/SA and PVA/SA/0.3M CaCO_3 hydrogel sheets to Cu^{2+} at different temperatures.

Table 1. The adsorption kinetic parameters of different models for PVA/SA and PVA/SA/0.3M CaCO_3 hydrogel sheets

Temperature (°C)	Hydrogels	Adsorption efficiency (%)	Pseudo-first-order			Pseudo-second-order		
			q_e ($\text{mg} \cdot \text{g}^{-1}$)	K_1 (min^{-1})	R^2	q_e ($\text{mg} \cdot \text{g}^{-1}$)	K_2 ($\text{g}/\text{mg} \cdot \text{min}$)	R^2
4	PVA/SA	47.58	6.870	0.0355	0.9667	7.3409	0.0072	0.9918
	PVA/SA/0.3M CaCO_3	86.00	12.9383	0.0311	0.9584	13.8633	0.00315	0.9940
20	PVA/SA	51.17	7.0185	0.0267	0.8631	7.9739	0.0045	0.9641
	PVA/SA/0.3M CaCO_3	92.04	13.8968	0.0233	0.9454	14.5770	0.0026	0.9670

	3M CaCO ₃							
	PVA/SA	46.54	6.1047	0.0649	0.9313	6.4266	0.0164	0.9521
40	PVA/SA/0.3M CaCO ₃	90.04	13.0048	0.0297	0.9838	14.9075	0.0024	0.9911
	3M CaCO ₃							

3.3.5. Adsorption isotherm studies

The adsorption isotherm is an important index to evaluate the adsorption relationship between the adsorbent and the adsorption surface at a certain temperature. The adsorption isotherms of PVA/SA and PVA/SA/0.3M CaCO₃ hydrogel sheets at 20 °C are shown in **Fig. 7**. The results showed that with the increase of the feeding ion concentration, the adsorption efficiency of Cu²⁺ of the two kinds of hydrogels increased significantly, and the color of the hydrogel sheets gradually changed from translucent (PVA/SA) and white (PVA/SA/0.3M CaCO₃) to light blue and greenish blue. Langmuir equation and Freundlich equation are currently the most popular for fitting adsorption isotherms, which are given as follows [48,49]:

$$\text{Langmuir equation: } q_e = \frac{Q_{max}K_L C_e}{1 + K_L C_e} \quad (7)$$

$$\text{Freundlich equation: } q_e = K_F C_e^{\frac{1}{n}} \quad (8)$$

Where q_e is the mass of solute adsorbed per unit sample at equilibrium (mg/g), Q_{max} is the adsorption capacity (mg/g), C_e is the equilibrium concentration of solution, K_L is the Langmuir model constant (L/mg), K_F is the Freundlich model constant (L/g), n is the anisotropic index [48,49].

Langmuir model is based on monolayer adsorption with uniform adsorption sites, while Freundlich model assumes unequal adsorption sites. From the perspective of R² value (**Table 2**), the adsorption of Cu²⁺ by PVA/SA and PVA/SA/0.3M CaCO₃ was more consistent with Langmuir model, indicating that the active sites of the two are uniform, and the adsorption of Cu²⁺ heavy metal ions is mainly monolayer adsorption. In addition, **Fig. 7c-d** showed that the adsorption efficiency of Cu²⁺ by PVA/SA decreased with the increase of ion concentration, and the three-hour adsorption efficiency curve was close to the equilibrium adsorption curve, indicating that a large degree of adsorption process was completed in 3h. However, there were some irregular phenomena in the equilibrium adsorption capacity of PVA/SA/0.3M CaCO₃ at low concentration, which was

most likely caused by low concentration difference effect between the surface of hydrogel and the media. In contrast, PVA/SA/0.3M CaCO₃ achieved the highest Cu²⁺ adsorption efficiency of > 90% at 640-1280 mg/L (0.01-0.02 mol/L), indicating that almost all Cu²⁺ was removed by the hydrogel in the media. Compared to PVA/SA, adsorption efficiency of PVA/SA/0.3M CaCO₃ was much higher, which meant that the addition of CaCO₃ effectively improved the adsorption of Cu²⁺ by hydrogels (Fig. 7 d).

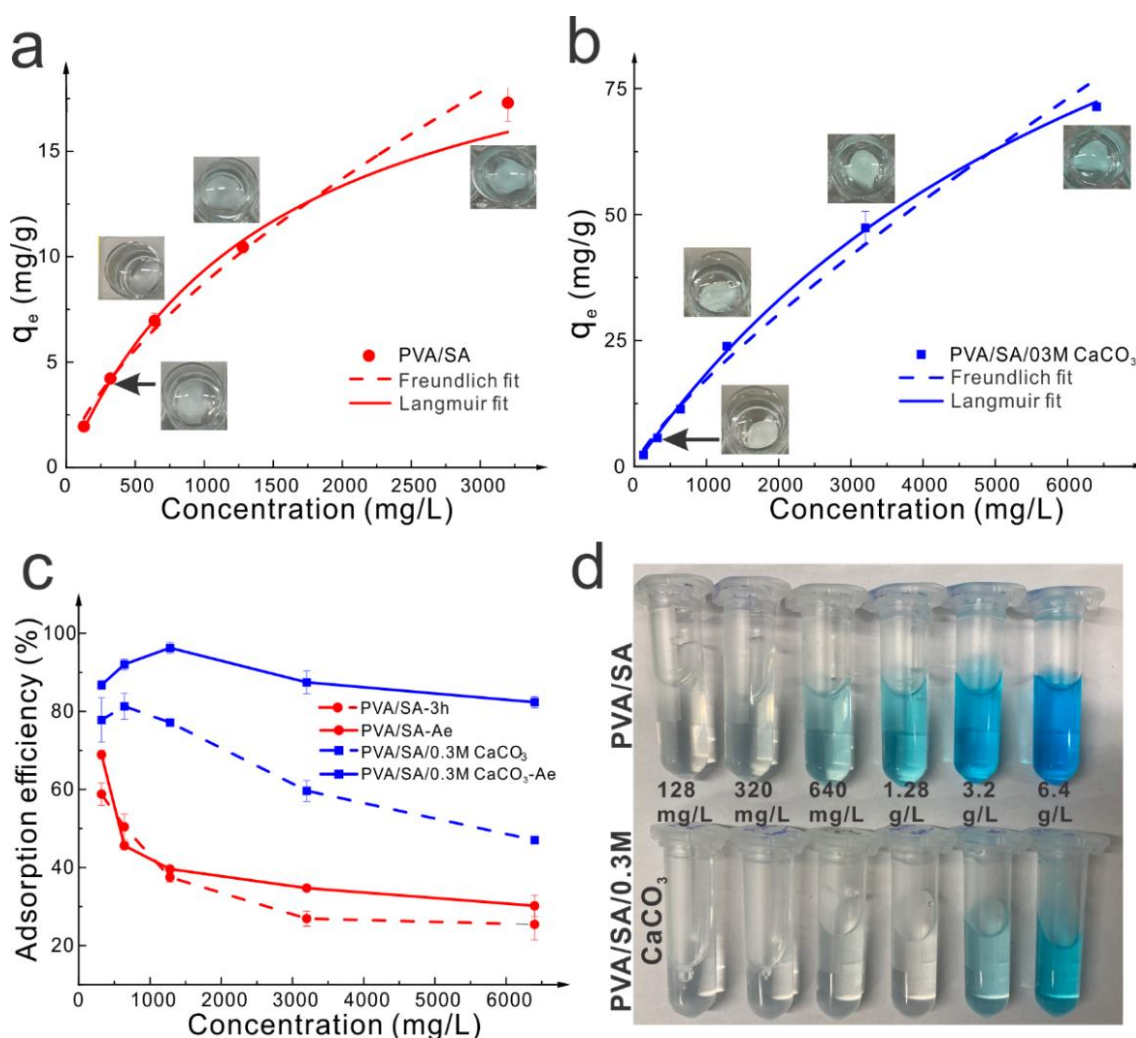


Fig. 7. The adsorption isotherms of PVA/SA and PVA/SA/0.3M CaCO₃ hydrogel sheets to Cu²⁺ at 20 °C. (a and b) Langmuir and Freundlich adsorption isotherm models, (c) 3 h adsorption efficiency and adsorption equilibrium of PVA/SA and PVA/SA/0.3M CaCO₃ hydrogel sheets to Cu²⁺ at different concentration media, (d) Sample images of chelated supernatant after 3 h adsorption.

Table 2. Adsorption isotherm parameters of Cu²⁺ by PVA/SA and PVA/SA/0.3M CaCO₃ hydrogel sheets.

Temperature (°C)	Hydrogels	Freundlich			Langmuir		
		1/n	$K_F(\text{mg/g})(\text{L/mg})^{1/n}$	R^2	Q_{\max} (mg/g)	K_L (L/mg)	R^2
20	PVA/SA	0.6458	1012	0.9921	23.35	6.687E ⁻⁴	0.9948
	PVA/SA/0.3M CaCO ₃	0.8023	0.0679	0.9773	157.7	1.325E ⁻⁴	0.9960

3.3.6. Adsorption thermodynamics

Adsorption thermodynamic parameters are of great significance for understanding the mechanism of adsorption process, optimizing adsorption conditions, and designing adsorption materials, which can be determined by the variation of adsorption equilibrium constant K_0 with temperature. The thermodynamic parameters of standard Gibbs free energy (ΔG^0 , kJ/mol), enthalpy (ΔH^0 , kJ/mol) and entropy (ΔS^0 , kJ/mol K) are determined by the following equations [50]:

$$\ln \left(\frac{q_e}{C_e} \right) = \frac{\Delta S}{R} - \frac{\Delta H}{RT} \quad (9)$$

$$\Delta G = \Delta H - T\Delta S \quad (10)$$

where ΔG , ΔH , and ΔS indicate the changes in Gibbs free energy (kJ/mol), enthalpy (kJ/mol), and entropy ($\text{J}\cdot\text{mol}^{-1}\cdot\text{K}^{-1}$), respectively; q_e , C_e , R , and T are the amount of Cu^{2+} adsorbed on the adsorbent of the solution at equilibrium (mg/L), the equilibrium concentration of Cu^{2+} in the solution (mg/L), the gas constant (8.314 $\text{J}\cdot\text{mol}^{-1}\cdot\text{K}^{-1}$), and the absolute temperature (K), respectively. The results are shown in **Table 3**, and the negative ΔG^0 and positive ΔH^0 indicated that the adsorption of Cu^{2+} by PVA/SA and PVA/SA/CaCO₃ was a spontaneous and endothermic process, and positive ΔS^0 indicated the increase of disorder at the solid/solution interface during the adsorption process [51]. It is worth noting that under the same conditions, the absolute values of ΔG^0 and ΔS^0 of PVA/SA/CaCO₃ were significantly higher than those of PVA/SA, which also indicated that the adsorption process of Cu^{2+} is more likely to occur in the former.

Table 3. Adsorption isotherm parameters of Cu^{2+} by PVA/SA and PVA/SA/0.3M CaCO₃ hydrogel sheets.

Temperature	Hydrogels	Heavy metal	ΔG^0 kJ/mol	ΔH^0 (kJ/mol)	ΔS^0 (J/mol·K)
-------------	-----------	-------------	---------------------	-----------------------	------------------------

(°C)					
4	PVA/SA		-1.49	1.96	5.38
	PVA/SA/0.3 M CaCO ₃		-1.84	0.93	9.97
20	PVA/SA	Cu ²⁺	-1.48	1.96	5.36
	PVA/SA/0.3 M CaCO ₃		-1.93	0.93	10.31
40	PVA/SA		-1.49	1.96	5.38
	PVA/SA/0.3 M CaCO ₃		-1.94	0.93	10.35

3.3.7 Adsorption mechanism

The adsorption mechanism of Cu²⁺ on PVA/SA and PVA/SA/CaCO₃ hydrogel sheets was analyzed, as shown in **Fig. 8**. It is well known that SA is a polycarboxylic acid polymer with abundant carboxyl functional groups, which has strong electrostatic interaction with metal Cu²⁺ ions. In addition, the lone electron pairs existing in -OH and -COOH groups in PVA/SA can be shared with Cu²⁺, which can form complexes or salts through reaction, promoting the preferential adsorption of Cu²⁺ on the surface of PVA/SA (**Fig. 8a**) [52]. Notably, due to the similar structure and charge properties of Cu²⁺ and Ca²⁺, the former tended to cause ionic crosslinking of hydrogels, which meant Cu²⁺ can serve as an ionic crosslinking agent to partially replace Ca²⁺ (**Fig. 8b**) [38,39]. The FTIR spectra of the PVA/SA before and after adsorption revealed no significant changes in the structure of the sheets (**Fig. 8c**). However, in the XRD spectra, the diffraction peaks of the sample after adsorption were significantly enhanced, indicating an increase in the crystallinity of the corresponding phase. This enhancement was attributed to the formation of complexes between the carboxylate in PVA/SA and free Cu²⁺. Particularly, distinct diffraction peaks appeared at 2θ=32.8°, 43.9°, 50.1° after adsorption tests. Compared with PVA/SA, the presence of CaCO₃ in PVA/SA/CaCO₃ not only increased the surface roughness to a certain extent, causing uneven charge distribution and more binding sites, but also provided anion ions with stronger ionization properties (CO₃²⁻), eventually led to higher adsorption efficiency. Specifically, in addition to the same adsorption mechanism as PVA/SA, the precipitation reaction caused by CO₃²⁻ ions occupy a dominant position in PVA/SA/CaCO₃, because we found that the color of films after adsorption tests turned aeruginous, and it became deeper with the increase of adsorption content [39]. This was reasonable since

precipitation reactions had a stronger propensity than other effects. The phase analysis of the reacted sample showed that the diffraction peak of the original vaterite became extremely sharp, and in the case of no vaterite added, it can only be judged as the formation of a copper salt compound with similar structural properties.

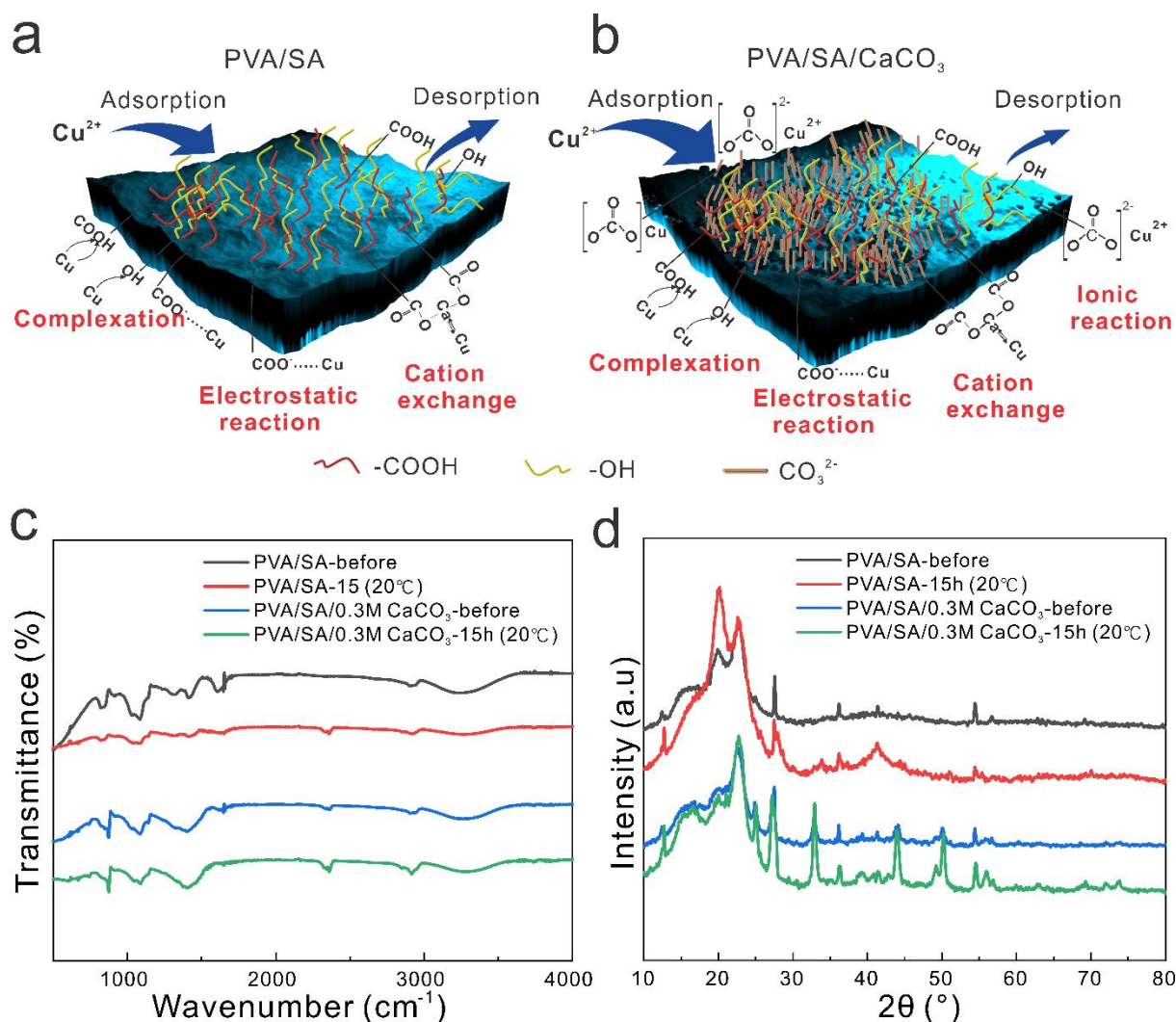


Fig. 8. (a and b) Adsorption mechanism of Cu^{2+} by PVA/SA and PVA/SA/ CaCO_3 ; (c and d) IR and XRD spectra of PVA/SA and PVA/SA/0.3M CaCO_3 hydrogel sheets before and after 3 h adsorption tests at 20 °C.

3.3.8 Regeneration and reusability study

The adsorbents were easily regenerated in 0.005 M HCl solution and distilled water, and their reusability performance for the removal of Cu^{2+} was analyzed by repeating adsorption-desorption cycle five times (20 °C), and the results is shown in **Fig. 9**. It can be seen that the Cu^{2+} removal efficiency of PVA/SA/0.3M CaCO_3

was still as high as more than 80% after 4 regeneration cycles, but with further cycles, the value dropped significantly, while that of PVA/SA maintained well. Apparently, this was because acid washing gradually decomposed CaCO_3 in the mixture, thereby reducing the adsorption efficiency. Nevertheless, the adsorption capacity of PVA/SA/0.3M CaCO_3 was still higher than that of PVA/SA. This confirmed the crucial role of CaCO_3 in Cu^{2+} removal process, and also stimulated the potential of composite materials formed by polymers combined with inorganic nanoparticles in the removal of heavy metal ions.

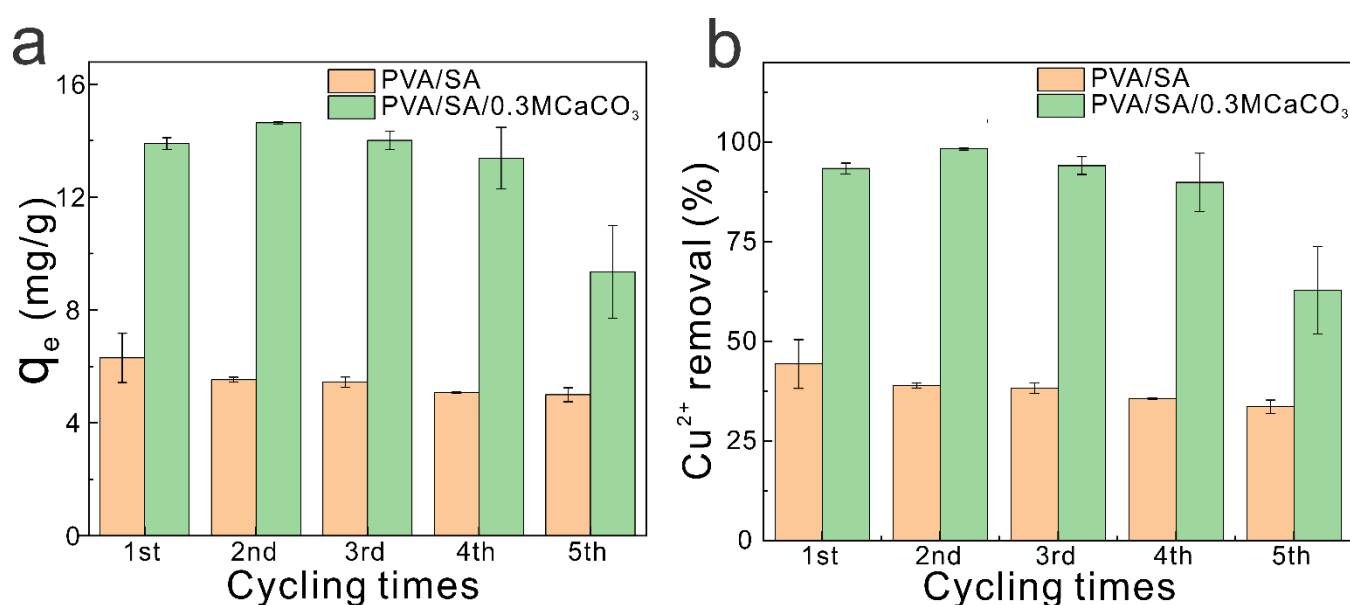


Fig. 9. (a and b) The relationship between the adsorption capacity (a) and removal rate (b) of Cu^{2+} by PVA/SA and PVA/SA/0.3 CaCO_3 and the number of cycles.

3.3.9 Comparison with other SA-based and PVA-based adsorbents

We compared the q_m of PVA/SA/ CaCO_3 composite hydrogel sheet with the reported q_m of SA or PVA-based adsorbents and other films (**Table 4**). Our self-assembled hydrogel sheet was able to adsorb Cu^{2+} more efficiently than other adsorbents, indicating its potential as an adsorbent for heavy metal ions. In addition, PVA/SA and PVA/SA/0.3M CaCO_3 were placed in simulated heavy metal ion wastewater (**Table S2**) for adsorption test [53]. Despite the competitive adsorption effect of many other heavy metal ions, PVA/SA/0.3M CaCO_3 still exhibited up to 70% removal efficiency of Cu^{2+} after impregnation at 20 °C for 15h, while it was

only $24 \pm 1.03\%$ for PVA/SA. Those results indicated that the PVA/SA/CaCO₃ composite hydrogel prepared in this study has a great potential application for wastewater purification.

Table 4. Comparison of the adsorption capacity of various adsorbents for Cu²⁺

Adsorbent	q _{max} (mg/g)	Ref.
Chitosan/PVA/ polyethyleneimine	86.08	[54]
Chitosan/calcium alginate/bentonite	115.30	[55]
Hydrazide-functionalized SA	157.1	[56]
Cu (II) ion-imprinted hydrogel	40.96	[57]
Cellulose/Hemicellulose/Lignin hydrogel	73.02	[58]
PVA hydrogel	14.41	[59]
Grafted guar gum hydrogel	90.3	[60]
Chitosan/carboxymethyl guar gum film	155.51	[61]
Acrylamide/acrylic acid cellulose hydrogel	157.51	[62]
Cellulose hydrogel	52.3	[63]
Xanthan gum/chitosan biofilm hydrogel	139.71	[64]
Cellulose nanofibril/chitosan hydrogel	148.30	[65]
PVA/SA/CaCO₃ hybrid hydrogel	157.7	This study

4. Conclusion

The PVA/SA/CaCO₃ hybrid hydrogel sheet was synthesized by a one-pot method, and the effects of CaCO₃ concentrations on the surface structure, mechanical properties, and Cu²⁺ ions adsorption capacity of the hydrogel sheet were explored. The results of SEM and AFM showed that the introduction of CaCO₃ increased the surface roughness of the PVA/SA hydrogel sheet and improved the adsorption nodes on the surface. Phase composition analysis showed the cross-linking state of PVA and SA in PVA/SA/ CaCO₃ and confirmed that CaCO₃ mainly existed in the form of 2-4 μm vaterite particles. The hydrogel films exhibited higher elongation due to the presence of CaCO₃, although their tensile strength decreased slightly with the increase of CaCO₃ content. The content of CaCO₃, time and temperature significantly affected the adsorption

rate, efficiency and adsorption kinetic of PVA/SA/CaCO₃ for Cu²⁺ ions. The introduction of CaCO₃ significantly accelerated the adsorption rate of Cu²⁺ on the hydrogel sheet, and obtained a saturated adsorption capacity twice that of PVA/SA. An increase in temperature accelerated the time for PVA/SA and PVA/SA/CaCO₃ to reach adsorption equilibrium and increased the saturation adsorption efficiency. Adsorption kinetics analysis showed that the adsorption of Cu²⁺ by PVA/SA and PVA/SA/CaCO₃ aligned more with the pseudo-second-order kinetic model, indicating that the adsorption process was more inclined to chemical adsorption than physical adsorption. The adsorption process conformed to Langmuir model with q_m of 157.7 mg/g, and thermodynamic analysis indicated that the adsorption process was spontaneous and exothermic. The highly efficient adsorption of Cu²⁺ ions by PVA/SA/CaCO₃ resulted from the synergistic adsorption mechanism of electrostatic interaction, complexation, cation exchange and ionic reaction. Regeneration experiment and comparative results showed that PVA/SA/CaCO₃ has greater application potential for wastewater purification.

Declaration of Competing Interest

The authors declare that they have no known competing financial interests or personal relationships that could have appeared to influence the work reported in this paper.

Acknowledgements

This research has been developed with support of FWO-F.N.R.S. under the Excellence of Science (EOS) program, grant number: 40007488. This work is also supported by EU project “SurfBio” grant no.: 952379.

We also thank the Flemish Research Council (FWO), I002620N, G043322N, and BOF-UGent: BOF14/IOP/003, BOF23/GOA/029. YH acknowledges support of the China Scholarship Council (CSC No. 202006370040).

Reference

- [1] D. Zhou, L. Zhang, J. Zhou, S. Guo, Cellulose/chitin beads for adsorption of heavy metals in aqueous solution, *Water Res.* 38 (2004) 2643–2650.
- [2] M.A. Stylianou, V.J. Inglezakis, K.G. Moustakas, S.P. Malamis, M.D. Loizidou, Removal of Cu(II) in fixed bed and batch reactors using natural zeolite and exfoliated vermiculite as adsorbents, *Desalination.* 215 (2007) 133–142. <https://doi.org/https://doi.org/10.1016/j.desal.2006.10.031>.
- [3] V.J.P. Vilar, C.M.S. Botelho, R.A.R. Boaventura, Copper desorption from Gelidium algal biomass, *Water Res.* 41 (2007) 1569–1579. <https://doi.org/https://doi.org/10.1016/j.watres.2006.12.031>.
- [4] P. Zhang, K. Zou, L. Yuan, J. Liu, B. Liu, T.-P. Qing, B. Feng, A biomass resource strategy for alginate-polyvinyl alcohol double network hydrogels and their adsorption to heavy metals, *Sep. Purif. Technol.* 301 (2022) 122050. <https://doi.org/https://doi.org/10.1016/j.seppur.2022.122050>.
- [5] S.N. Basri, N. Zainuddin, K. Hashim, N.A. Yusof, Preparation and characterization of irradiated carboxymethyl sago starch-acid hydrogel and its application as metal scavenger in aqueous solution, *Carbohydr. Polym.* 138 (2016) 34–40. <https://doi.org/https://doi.org/10.1016/j.carbpol.2015.11.028>.
- [6] R.C. Bansal, M. Goyal, Activated carbon adsorption, CRC press, 2005.
- [7] R.O. James, T.W. Healy, Adsorption of hydrolyzable metal ions at the oxide—water interface. I. Co (II) adsorption on SiO₂ and TiO₂ as model systems, *J. Colloid Interface Sci.* 40 (1972) 42–52.
- [8] Y. Guo, H. Lu, F. Zhao, X. Zhou, W. Shi, G. Yu, Biomass-derived hybrid hydrogel evaporators for cost-effective solar water purification, *Adv. Mater.* 32 (2020) 1907061.
- [9] R. Xu, G. Zhou, Y. Tang, L. Chu, C. Liu, Z. Zeng, S. Luo, New double network hydrogel adsorbent: Highly efficient removal of Cd(II) and Mn(II) ions in aqueous solution, *Chem. Eng. J.* 275 (2015) 179–188. <https://doi.org/https://doi.org/10.1016/j.cej.2015.04.040>.
- [10] S. Thakur, P.P. Govender, M.A. Mamo, S. Tamulevicius, V.K. Thakur, Recent progress in gelatin

- hydrogel nanocomposites for water purification and beyond, *Vacuum*. 146 (2017) 396–408.
- [11] Y. Guo, J. Bae, Z. Fang, P. Li, F. Zhao, G. Yu, Hydrogels and hydrogel-derived materials for energy and water sustainability, *Chem. Rev.* 120 (2020) 7642–7707.
- [12] M.R. Guilherme, A. V Reis, A.T. Paulino, A.R. Fajardo, E.C. Muniz, E.B. Tambourgi, Superabsorbent hydrogel based on modified polysaccharide for removal of Pb²⁺ and Cu²⁺ from water with excellent performance, *J. Appl. Polym. Sci.* 105 (2007) 2903–2909.
- [13] Y. Huang, L. Cao, B. V Parakhonskiy, A.G. Skirtach, Hard, Soft, and Hard-and-Soft Drug Delivery Carriers Based on CaCO₃ and Alginate Biomaterials: Synthesis, Properties, Pharmaceutical Applications, *Pharm.* . 14 (2022). <https://doi.org/10.3390/pharmaceutics14050909>.
- [14] X. Gao, C. Guo, J. Hao, Z. Zhao, H. Long, M. Li, Adsorption of heavy metal ions by sodium alginate based adsorbent-a review and new perspectives, *Int. J. Biol. Macromol.* 164 (2020) 4423–4434.
- [15] C.K. Kuo, P.X. Ma, Ionically crosslinked alginate hydrogels as scaffolds for tissue engineering: Part 1. Structure, gelation rate and mechanical properties, *Biomaterials*. 22 (2001) 511–521.
- [16] A. Kumar, S.S. Han, PVA-based hydrogels for tissue engineering: A review, *Int. J. Polym. Mater. Polym. Biomater.* 66 (2017) 159–182.
- [17] J. Wei, Y. Zhao, S. Yu, J. Du, X. Hu, G. Bai, Z. Wang, Environment-friendly dual-network hydrogel dust suppressant based on xanthan gum, polyvinyl alcohol and acrylic acid, *J. Environ. Manage.* 295 (2021) 113139. <https://doi.org/https://doi.org/10.1016/j.jenvman.2021.113139>.
- [18] P.J. Martens, S.J. Bryant, K.S. Anseth, Tailoring the degradation of hydrogels formed from multivinyl poly (ethylene glycol) and poly (vinyl alcohol) macromers for cartilage tissue engineering, *Biomacromolecules*. 4 (2003) 283–292.
- [19] Y. Zhang, M. Jiang, Y. Zhang, Q. Cao, X. Wang, Y. Han, G. Sun, Y. Li, J. Zhou, Novel lignin–chitosan–PVA composite hydrogel for wound dressing, *Mater. Sci. Eng. C*. 104 (2019) 110002.

- [20] E.A. Kamoun, E.-R.S. Kenawy, X. Chen, A review on polymeric hydrogel membranes for wound dressing applications: PVA-based hydrogel dressings, *J. Adv. Res.* 8 (2017) 217–233.
- [21] L. Jin, R. Bai, Mechanisms of lead adsorption on chitosan/PVA hydrogel beads, *Langmuir.* 18 (2002) 9765–9770.
- [22] L.-Y. Wang, M.-J. Wang, Removal of heavy metal ions by poly (vinyl alcohol) and carboxymethyl cellulose composite hydrogels prepared by a freeze–thaw method, *ACS Sustain. Chem. Eng.* 4 (2016) 2830–2837.
- [23] J.H. Chen, G.P. Li, Q.L. Liu, J.C. Ni, W.B. Wu, J.M. Lin, Cr(III) ionic imprinted polyvinyl alcohol/sodium alginate (PVA/SA) porous composite membranes for selective adsorption of Cr(III) ions, *Chem. Eng. J.* 165 (2010) 465–473. <https://doi.org/https://doi.org/10.1016/j.cej.2010.09.034>.
- [24] X. Yi, F. Sun, Z. Han, F. Han, J. He, M. Ou, J. Gu, X. Xu, Graphene oxide encapsulated polyvinyl alcohol/sodium alginate hydrogel microspheres for Cu (II) and U (VI) removal, *Ecotoxicol. Environ. Saf.* 158 (2018) 309–318. <https://doi.org/https://doi.org/10.1016/j.ecoenv.2018.04.039>.
- [25] M.-K. Zhang, X.-H. Zhang, G.-Z. Han, Magnetic alginate/PVA hydrogel microspheres with selective adsorption performance for aromatic compounds, *Sep. Purif. Technol.* 278 (2021) 119547. <https://doi.org/https://doi.org/10.1016/j.seppur.2021.119547>.
- [26] J. Wang, S. Zheng, Y. Shao, J. Liu, Z. Xu, D. Zhu, Amino-functionalized Fe₃O₄@ SiO₂ core–shell magnetic nanomaterial as a novel adsorbent for aqueous heavy metals removal, *J. Colloid Interface Sci.* 349 (2010) 293–299.
- [27] S.M. Al-Jubouri, H.A. Sabbar, H.A. Lafta, B.I. Waisi, Effect of synthesis parameters on the formation 4A zeolite crystals: characterization analysis and heavy metals uptake performance study for water treatment, *Desalin. Water Treat.* 165 (2019) 290–300.
- [28] L. Roshanfekar Rad, M. Anbia, Zeolite-based composites for the adsorption of toxic matters from water:

- A review, *J. Environ. Chem. Eng.* 9 (2021) 106088.
<https://doi.org/https://doi.org/10.1016/j.jece.2021.106088>.
- [29] B. V. Parakhonskiy, A. Haase, R. Antolini, Sub-micrometer vaterite containers: Synthesis, substance loading, and release, *Angew. Chemie - Int. Ed.* 51 (2012) 1195–1197.
<https://doi.org/10.1002/anie.201104316>.
- [30] A.G. Christy, A review of the structures of vaterite: the impossible, the possible, and the likely, *Cryst. Growth Des.* 17 (2017) 3567–3578.
- [31] S. Sovova, A. Abalymov, M. Pekar, A.G. Skirtach, B. Parakhonskiy, Calcium carbonate particles: synthesis, temperature and time influence on the size, shape, phase, and their impact on cell hydroxyapatite formation, *J. Mater. Chem. B.* 9 (2021) 8308–8320. <https://doi.org/10.1039/d1tb01072g>.
- [32] Y.I.I. Svenskaya, H. Fattah, O.A.A. Inozemtseva, A.G.G. Ivanova, S.N.N. Shtykov, D.A.A. Gorin, B.V. V Parakhonskiy, Key Parameters for Size- and Shape-Controlled Synthesis of Vaterite Particles, *Cryst. Growth Des.* 18 (2018) 331–337. <https://doi.org/10.1021/acs.cgd.7b01328>.
- [33] P.-Y. Lin, H.-M. Wu, S.-L. Hsieh, J.-S. Li, C. Dong, C.-W. Chen, S. Hsieh, Preparation of vaterite calcium carbonate granules from discarded oyster shells as an adsorbent for heavy metal ions removal, *Chemosphere.* 254 (2020) 126903.
- [34] P.M. Schosseler, B. Wehrli, A. Schweiger, Uptake of Cu²⁺ by the calcium carbonates vaterite and calcite as studied by continuous wave (cw) and pulse electron paramagnetic resonance, *Geochim. Cosmochim. Acta.* 63 (1999) 1955–1967. [https://doi.org/https://doi.org/10.1016/S0016-7037\(99\)00086-1](https://doi.org/https://doi.org/10.1016/S0016-7037(99)00086-1).
- [35] J. Kontrec, D. Kralj, L. Brečević, G. Falini, Influence of some polysaccharides on the production of calcium carbonate filler particles, *J. Cryst. Growth.* 310 (2008) 4554–4560.
<https://doi.org/https://doi.org/10.1016/j.jcrysgr.2008.07.106>.

- [36] I.N. Jasem, H.H. Abdullah, M. Jalal Abdulrazzaq, Dual-wavelength passively Q-switched erbium-doped fiber laser incorporating calcium carbonate nanoparticles as saturable absorber, *J. Nanotechnol.* 2023 (2023).
- [37] A. Hattali, O. Bouras, S. Hanini, Removal of cadmium from aqueous solution by hybrid reinforced porous gelled beads based on SA/PVA/Al-MT and CaCO₃., (2022).
- [38] Y. Zhang, L. Zhang, R. Gao, L. Zhong, J. Xue, CaCO₃-coated PVA/BC-based composite for the simultaneous adsorption of Cu(II), Cd(II), Pb(II) in aqueous solution, *Carbohydr. Polym.* 267 (2021) 118227. <https://doi.org/https://doi.org/10.1016/j.carbpol.2021.118227>.
- [39] K. Ahmad, I.A. Bhatti, M. Muneer, M. Iqbal, Z. Iqbal, Removal of heavy metals (Zn, Cr, Pb, Cd, Cu and Fe) in aqueous media by calcium carbonate as an adsorbent, *Int. J. Chem. Biochem. Sci.* 2 (2012) 48–53.
- [40] N. Stanley, B. Mahanty, Preparation and characterization of biogenic CaCO₃-reinforced polyvinyl alcohol–alginate hydrogel as controlled-release urea formulation, *Polym. Bull.* 77 (2020) 529–540.
- [41] D. Jahani, A. Nazari, J. Ghourbanpour, A. Ameli, Polyvinyl alcohol/calcium carbonate nanocomposites as efficient and cost-effective cationic dye adsorbents, *Polymers (Basel)*. 12 (2020) 2179.
- [42] S. Tang, J. Yang, L. Lin, K. Peng, Y. Chen, S. Jin, W. Yao, Construction of physically crosslinked chitosan/sodium alginate/calcium ion double-network hydrogel and its application to heavy metal ions removal, *Chem. Eng. J.* 393 (2020) 124728. <https://doi.org/https://doi.org/10.1016/j.cej.2020.124728>.
- [43] H. Ren, Z. Gao, D. Wu, J. Jiang, Y. Sun, C. Luo, Efficient Pb(II) removal using sodium alginate–carboxymethyl cellulose gel beads: Preparation, characterization, and adsorption mechanism, *Carbohydr. Polym.* 137 (2016) 402–409. <https://doi.org/https://doi.org/10.1016/j.carbpol.2015.11.002>.
- [44] J.M. Didymus, P. Oliver, S. Mann, A.L. DeVries, P. V Hauschka, P. Westbroek, Influence of low-molecular-weight and macromolecular organic additives on the morphology of calcium carbonate, *J.*

- Chem. Soc. Faraday Trans. 89 (1993) 2891–2900.
- [45] Y.-Q. Niu, J.-H. Liu, C. Aymonier, S. Fermani, D. Kralj, G. Falini, C.-H. Zhou, Calcium carbonate: Controlled synthesis, surface functionalization, and nanostructured materials, *Chem. Soc. Rev.* 51 (2022) 7883–7943.
- [46] S. Lagergren, Zur theorie der sogenannten adsorption geloster stoffe, *K. Sven. Vetenskapsakademiens. Handl.* 24 (1898) 1–39.
- [47] Y.S. Ho, G. McKay, Pseudo-second order model for sorption processes, *Process Biochem.* 34 (1999) 451–465. [https://doi.org/https://doi.org/10.1016/S0032-9592\(98\)00112-5](https://doi.org/https://doi.org/10.1016/S0032-9592(98)00112-5).
- [48] J.C. Crittenden, R.R. Trussell, D.W. Hand, K.J. Howe, G. Tchobanoglous, *MWH's water treatment: principles and design*, John Wiley & Sons, 2012.
- [49] J. Edzwald, *Water quality & treatment: a handbook on drinking water*, McGraw-Hill Education, 2011.
- [50] V.K. Gupta, A. Mittal, L. Krishnan, V. Gajbe, Adsorption kinetics and column operations for the removal and recovery of malachite green from wastewater using bottom ash, *Sep. Purif. Technol.* 40 (2004) 87–96. <https://doi.org/https://doi.org/10.1016/j.seppur.2004.01.008>.
- [51] L. Wang, J. Zhang, R. Zhao, C. Li, Y. Li, C. Zhang, Adsorption of basic dyes on activated carbon prepared from *Polygonum orientale* Linn: Equilibrium, kinetic and thermodynamic studies, *Desalination.* 254 (2010) 68–74. <https://doi.org/https://doi.org/10.1016/j.desal.2009.12.012>.
- [52] W. Zhang, Q. Deng, Q. He, J. Song, S. Zhang, H. Wang, J. Zhou, H. Zhang, A facile synthesis of core-shell/bead-like poly (vinyl alcohol)/alginate@PAM with good adsorption capacity, high adaptability and stability towards Cu(II) removal, *Chem. Eng. J.* 351 (2018) 462–472. <https://doi.org/https://doi.org/10.1016/j.cej.2018.06.129>.
- [53] M. Henze, Y. Comeau, Wastewater characterization, *Biol. Wastewater Treat. Princ. Model. Des.* 27 (2008).

- [54] N. Sahebamee, M. Soltanieh, S.M. Mousavi, A. Heydarinasab, Removal of Cu²⁺, Cd²⁺ and Ni²⁺ ions from aqueous solution using a novel chitosan/polyvinyl alcohol adsorptive membrane, *Carbohydr. Polym.* 210 (2019) 264–273.
- [55] Z. Lin, Y. Yang, Z. Liang, L. Zeng, A. Zhang, Preparation of chitosan/calcium alginate/bentonite composite hydrogel and its heavy metal ions adsorption properties, *Polymers (Basel)*. 13 (2021) 1891.
- [56] T. Shi, Z. Xie, X. Mo, Y. Feng, T. Peng, D. Song, Highly efficient adsorption of heavy metals and cationic dyes by smart functionalized sodium alginate hydrogels, *Gels*. 8 (2022) 343.
- [57] J. Wang, L. Ding, J. Wei, F. Liu, Adsorption of copper ions by ion-imprinted simultaneous interpenetrating network hydrogel: Thermodynamics, morphology and mechanism, *Appl. Surf. Sci.* 305 (2014) 412–418. <https://doi.org/10.1016/j.apsusc.2014.03.102>.
- [58] S. Shan, X.-F. Sun, Y. Xie, W. Li, T. Ji, High-Performance Hydrogel Adsorbent Based on Cellulose, Hemicellulose, and Lignin for Copper(II) Ion Removal, *Polymers (Basel)*. 13 (2021). <https://doi.org/10.3390/polym13183063>.
- [59] T. Jamnongkan, A. Wattanakornsiri, P. Wachirawongsakorn, S. Kaewpirom, Effects of crosslinking degree of poly(vinyl alcohol) hydrogel in aqueous solution: kinetics and mechanism of copper(II) adsorption, *Polym. Bull.* 71 (2014) 1081–1100. <https://doi.org/10.1007/s00289-014-1112-7>.
- [60] A.E. Mubark, H.A. Hakem, E.G. Zaki, S.M. Elsaed, A.A.-H. Abdel-Rahman, Sequestration of Cd(II) and Cu(II) ions using bio-based hydrogel: a study on the adsorption isotherms and kinetics, *Int. J. Environ. Sci. Technol.* 19 (2022) 10877–10892. <https://doi.org/10.1007/s13762-021-03857-3>.
- [61] A. Rahmatpour, N. Alijani, An all-biopolymer self-assembling hydrogel film consisting of chitosan and carboxymethyl guar gum: A novel bio-based composite adsorbent for Cu²⁺ adsorption from aqueous solution, *Int. J. Biol. Macromol.* 242 (2023) 124878.
- [62] B. Zhao, H. Jiang, Z. Lin, S. Xu, J. Xie, A. Zhang, Preparation of acrylamide/acrylic acid cellulose

- hydrogels for the adsorption of heavy metal ions, *Carbohydr. Polym.* 224 (2019) 115022.
<https://doi.org/https://doi.org/10.1016/j.carbpol.2019.115022>.
- [63] Y.H. Teow, L.M. Kam, A.W. Mohammad, Synthesis of cellulose hydrogel for copper (II) ions adsorption, *J. Environ. Chem. Eng.* 6 (2018) 4588–4597.
<https://doi.org/https://doi.org/10.1016/j.jece.2018.07.010>.
- [64] A. Rahmatpour, A.H. Alizadeh, Biofilm hydrogel derived from physical crosslinking (self-assembly) of xanthan gum and chitosan for removing Cd²⁺, Ni²⁺, and Cu²⁺ from aqueous solution, *Int. J. Biol. Macromol.* 266 (2024) 131394. <https://doi.org/https://doi.org/10.1016/j.ijbiomac.2024.131394>.
- [65] X. Chen, Z. Song, B. Yuan, X. Li, S. Li, T. Thang Nguyen, M. Guo, Z. Guo, Fluorescent carbon dots crosslinked cellulose Nanofibril/Chitosan interpenetrating hydrogel system for sensitive detection and efficient adsorption of Cu (II) and Cr (VI), *Chem. Eng. J.* 430 (2022) 133154.
<https://doi.org/https://doi.org/10.1016/j.cej.2021.133154>.